Biomedical Signal Processing and Control 79 (2023) 104187

Contents lists available at ScienceDirect

Biomedical Signal Processing and Control

journal homepage: www.elsevier.com/locate/bspc

Toward an automatic detection of cardiac structures in short and long axis views

Laidi Amel [a], Mohammed Ammar [b,*], Mostafa El Habib Daho [c], Said Mahmoudi [d]

[a] Faculty of Engineering, LIMOSE Laboratory, M'Hamed Bougara University, Boumerdes, Algeria
[b] Engineering Systems and Telecommunication Laboratory, University M'Hamed Bougara, Boumerdes, Algeria
[c] Faculty of Technology, Biomedical Engineering Laboratory Abou Bekr Belkaid University, Tlemcen, Algeria
[d] University of Mons, Faculty of Engineering, Computer Science Department, 20 Place du parc, Mons B-7000, Belgium

ARTICLE INFO

Keywords:
Cardiac MRI Segmentation
Shape Descriptors
Particle Swarm Optimization
Residual Network
Interpretability

ABSTRACT

Objective: This work aims to create an automatic detection process of cardiac structures in both short-axis and long-axis views. A workflow inspired by human thinking process, for better explainability.
Methods: we began by separating the images into two classes: long axis and short axis, using a Residual Network model. Then, we used Particle Swarm Optimization for general segmentation. After segmentation, a characterization step based on shape descriptors calculated from bounding box and ANOVA for features selection were applied on the binary images to detect the location of each region of interest: lung, left and right ventricle in the short-axis view, the aorta, the left heart (left atrium and ventricle), and the right heart (right atrium and ventricle) in the long axis view.
Results: we achieved a 90% accuracy on view separation. We have selected: Elongation, Compactness, Circularity, Type Factor, for short axis identification; and:Area, Centre of Mass Y, Moment of Inertia XY, Moment of Inertia YY, for long axis identification.
Conclusion: a successful separation of long axis and short axis views allows for a better characterization and detection of segmented cardiac structures. After that, any method can be applied for segmentation, attribute selection, and classification.
Significance: an attempt to introduce explainability into cardiac image segmentation, we tried to mimic the human workflow while computerizing each step. The process seems to be valid and added clarity and interpretability to the detection.

1. Introduction

Despite all research and resources dedicated to cardiac diseases, they still are the leading cause of deaths around the globe. Automatic segmentation and characterization of structures of interest in cardiac MRI is an important step for understanding cardiac function and detecting malformations and cardiovascular diseases.

Many studies have been proposed to localize or detect the left ventricle (LV) and right ventricle (RV) in cardiac images.

The localization of cardiac structures can serve two different purposes:

- The automation of segmentation algorithms that require manual initialization. Such as methods based on active contours, level set, Active Shape Model (ASM), or Active Appearance Models (AAM).
- Characterization of regions after a global segmentation algorithm to isolate each region.

Image processing localization methods are classified into two categories:

1. The first category is based on the time variation; this approach exploits the movement of the heart during the cardiac cycle [1,2,3].

2. The second category is based on shape recognition [4,5].

The left ventricle has been the most investigated structure; early segmentation methods relied on low-level techniques like thresholding followed by a region-growing method. For instance, the authors in [6]

* Corresponding author.
E-mail addresses: a.laidi@univ-boumerdes.dz (L. Amel), m.ammar@univ-boumerdes.dz (M. Ammar), Said.Mahmoudi@umons.ac.be (S. Mahmoudi).

https://doi.org/10.1016/j.bspc.2022.104187
Received 4 September 2021; Received in revised form 27 July 2022; Accepted 4 September 2022
Available online 13 September 2022

separated the blood pool from the myocardium with a simple threshold, then used radial region-growing and convex hulling extraction to distinguish endocardial and epicardial boundaries. While in [7] thresholding was used to extract a region of interest for the left ventricle, and then it was followed by a region-growing step for segmentation of LV endocardium, epicardium, papillary muscles and trabeculations. In [8] the authors extracted the endocardium by initializing a level set segmentation method with a mask they get from thresholding. similarly, in [9] authors delineated the myocardial contours by first localising the LV in a previously thresholded image, they then used a segmentation method that is a fusion between intensity-based and texture-based fuzzy affinity maps, which is inspired by another fuzzy connectedness region-growing method [10]. The proposed method starts with setting a seed point and a sample region for the fuzzy connectedness estimates, which then gets expanded to using adaptive weights for the homogeneity and the gradient energy functions. The framework is finally extended to allow forces from dual contrast and fuzzy connectedness data integrated with shape constraints.

As for segmentation of the right ventricle, it remains a rather challenging task due to its irregular shape; It has mostly been done based on a joined segmentation with the left ventricle, taking advantage of the resemblance of texture in both blood cavities and the consistence of relative positions of both ventricles. Such information can come handy when working with active contours ([11,12]) or graph cut based methods [13]. It can also be used in frameworks that require prior information in the shape of a biomechanical model [14], a 3D heart model [15 16], or atlases ([17]), [18]).

With the emergence of deep learning, a lot of work focused on its application in cardiology [19]. even though deep learning-based methods achieved state of the art results, they still struggle with the issue of explainability. Most end to end deep learning models lack clarity and are considered black boxes, so they can hardly be trusted in critical applications.

As a compromise, recent papers explored combining deep learning with image processing methods; the authors in [20] used a structured inference on a deep belief network (DBN) to detect the left ventricle region of interest, then used that region as initialization for endocardium segmentation using Otsu's thresholding [21] and distance regularized level set. the final segmentation is used as an initial rough delineation for epicardium detection. They finally take the ROI detection to initialize an optimization process, and the delineation of the endocardial and epicardial borders to constrain a level set evolution.

In [22], the authors achieved high quality segmentations using a pipeline consisting of a distance regularized level-set method following a Deep Belief Network (DBNs) for both localization and segmentation of the left ventricle. while the authors in [23] they used a three-stage approach, starting with a Convolutional Neural Network CNN to detect the left ventricle chamber, then applied stacked autoencoder to infer the shape of the left ventricle, followed by level-set refinement. Luo et al. [24] adopted an LV atlas mapping method to achieve accurate localization using MRI data, then trained a three-layer CNN to predict the left ventricle.

The authors in [25] combined CNN with active contours, they used a four layer patch-based CNN to predict a vector starting from the evolving contour towards the closest point on the boundary of the object of interest, the set of predictions result in a vector field which was then used for evolving the contour through the Sobolev active contour framework.

Other studies involved Atlas-based methods. For instance, the authors in [26] came up with a novel encoder-decoder network called SVF-Net [27] and used it as a registration method for multi-atlas framework, which means they establishing predictions of the parameters from training images instead of the optimization of an energy criteria. Similarly, the authors in [28] reported achieving better accuracy compared to majority voting, patch-based label fusion, multi-atlas patch match and SVM with augmented features. They used deep learning for feature extraction and label fusion from cardiac MRI images, and then applied learned features to define a similarity measure for MRI atlas selection.

In a recent paper [29], the authors proposed a novel approach for ventricle localization using slope difference distribution (SDD) clustering and a coarse-to-fine SDD threshold selection method to locate the positions of the left and right ventricles. They begin by segmenting the ventricles in the first images of all the slices using the coarse SDD, all segmenting results are then added to form a grayscale image, the coarse SDD algorithm is then set to isolate a relatively high threshold in order to isolate two distinguish blobs that will be serve as seeds for left ventricle and right ventricle. Then seeded region growing is used to segment the LV and the RV in the first image of each slice. The coarse SDD threshold selection is used to obtain the coarse threshold for the generated RV and LV ROIs, while the fine SDD threshold selection is used to obtain the fine threshold for the same ROIs. They finally use post-processing to refine segmentation. The method achieved 100% localization accuracy for LV and 90% accuracy for RV, which exceeds any other state of the art results.

Noothout et al. [30] proposed a joint classification and regression based fully FCN (convolutional neutral network) to predict heart tissue anatomy landmark locations, where only those patches that are classified by the network as containing the landmark are used to determine the final landmark location.

Mahapatra [31] uses classification on local patches to find landmark regions, they focus their work inside ROIs to reduce the computational cost.

In this article, we ALSO combine deep learning with other image processing techniques in an automatic workflow for segmentation and characterization of the left and right ventricles from cardiac MRI images. The idea is to consider the thinking process executed by an expert, from seeing an MRI image until visually localizing the structures, and translating each step into an automatic process.

We begin by separating long-axis views from short-axis views using a deep learning network called Residual Network, and then we use Particle Swarm Optimization for general segmentation of different region of interest: lung, left and right ventricle in the short-axis view, the aorta, the left heart (left atrium and ventricle), and the right heart (right atrium and ventricle) in the long axis view. Finally, we propose characterizing the left and right ventricles using descriptors carefully chosen with an Analysis of variance (ANOVA). The rest of this paper includes a detailed description of the methods and materials used in this work in section 2, followed by the results found in each step of section 3, and finally a conclusion.

2. Materials and methods

2.1. Neural networks and Residual networks

Resnet or residual network is an artificial neural network. Neural networks are computing systems that rely on learning patterns and relationships from data through experience and error optimization instead of programing.

The learning process within artificial neural networks is a result of altering the network's weights at every iteration until the classification hits a perfect accuracy. Such a process demands a lot of images, in the order of millions, and a long training time.

Lately a new concept is introduced "transfer learning", where models are trained on very big datasets, has their weights frozen, then used on new tasks. They only need to be retrained on the desired task for a short period.

2.2. Particle swarm optimization

Particle Swarm Optimization (PSO) is another algorithm inspired from nature, proposed by Kennedy and Eberhart [32]. It is an optimization method based on the rules followed by groups of living organisms

to self-organise and act as a unit. It follows a set of regulations:

- Cohesion: particles tend to be drawn to the centre of the group.
- Alignment: particles follow the same path as their neighbours.
- Separation: to avoid collisions, particles self-separate with safety distance.

The Particle Swarm Optimization method assumes one important principle: there is no random movement, all particles have an objective to reach; this is determined by an "objective function" which should be either optimized or provided by the user, depending on the application at hand. This algorithm is used to solve multilevel thresholding segmentation problems, it has recently gained a reputation for providing perfect segmentation. In a recent publication [33], the others compared Particle Swarm Optimization for segmentation to the Ostu method, only to conclude that PSO-based image segmentation can create segments with great details. A similar approach by [34] used multimodal particle swarm optimization algorithm, which showed effectiveness and robustness and performed better than c-means.

Problem **formulation** [35]**:**

Image segmentation can be simplified as a binarization that keeps the target object, in our case the right and left ventricles, and eliminates everything else as background. Finding the right threshold to binarize an image is the most challenging part. In this work we estimate that the ideal threshold is calculated by maximizing the variance inter-class, defined by the following equation:

$$\sigma_B^2 \sum_{j=1}^{n} \omega_j \left(\mu_j - \mu_T\right)^2 \tag{1}$$

where j signifies a particular class, w_j is the probability of occurrence, and μ_j is the mean of class j.

The total mean of an image, or a particular class, can be calculated using its probability distribution, as shown on equation (2).

$$\mu_T = \sum^{L} i p_i \tag{2}$$

A probability distribution is a statistical function that describes the values that a variable can take within a given range, with the probabilities of the occurrences. It can be calculated with the formula (3).

$$p_i = \frac{h_i^c}{N}, \sum^{N} i = 1, p_i = 1 \tag{3}$$

Where:

I is a specific intensity value between [0, L-1].

N is the overall number of pixels in the image.

$\boldsymbol{h_i}$ is the number of pixels with intensity level *i*.

Finally, the thresholding problem is handled as an optimization aiming to find t_j , the threshold that maximizes the objective functions (fitness function) defined as:

$$1\varphi = max_{1<t_1<\cdots<t_{n-1}<L} \sigma_{\beta}^2(t_j) \tag{4}$$

In each step *t*, the particle success is controlled by a fitness function. As an imitation of the swarm [32], each particle n is considered in constant movement with coordinates $(x_n[t], v_n[t])$, where $0 \le x_n[t] \le$ L-1, and $(v_n[t])$ respectively are the position and velocity values, they rely highly on local best $(\check{x}_n[t])$ and global best $(\check{g}_n[t])$ information:

$$v_n[t+1] = \omega v_n[t] + \rho_1 r_1 \left(\check{g}_n - x_n\right) + \rho_2 r_2 \left(\check{x}_n - x_n[t]\right) \tag{5}$$

$$x_n[t+1] = x_n[t] + v_n[t+1]$$

The inertial influence is controlled by w, ρ_1 and ρ_2. It is usually set a value a little under 1. While the "cognitive" and "social" components are represented by r_1 and r_2 respectively.

2.3. Characterization of the right and left ventricle

The characterization step is very important. It allows the detection and localization of cardiac chambers like the left and right ventricles. A lot of different descriptors exist in the field of pattern recognition, choosing the right descriptors for a particular task depends on the nature of the object characterized.

Both ventricles have similar natures when it comes to texture and grayscale levels; a threshold segmentation method would result in the segmentation of both ventricles. However, the two ventricles have their differences; the left ventricle generally has a circular shape, and the right ventricle is longer, they also have distinguished spatial positions. That's why we choose to work with shape factors to differentiate between the two [36].

Shape factors are numerical values that depict the physical and spatial form of an object, regardless of its size.

2.3.1. Circularity factor :

Circularity factor is the most common shape describer, it compares the object to a circle. A circularity factor of 1 is addressed to a circle, the further the shape gets from a circle the smaller the value gets. It can be calculated in function of the perimeter P(R), and area A(R).

$$\boldsymbol{FcH} = P(R)/(2\sqrt{\pi A(R)} \tag{6}$$

2.3.2. Elongation factor

A less commonly used shape factor. Elongation factor, as its name suggests, calculates the elongation of the object. Suppose there is a bounding box rectangle surrounding the object, elongation is given as the ration between its width and length. The elongation value varies between 0 and 1, 1 being assigned to more of a circular or rectangular shape, as the ratio approaches 0, the shape resembles more of a long rectangle.

Elongation = Length $_{\text{bounding\_box}}$ / width $_{\text{bounding\_box}}$ (7).

2.3.3. Type Factor:

A feature linking the surface area to the moment of inertia.

$$\boldsymbol{F_t} = \frac{A^2}{4\pi\sqrt{I_{xx} + I_{yy}}} \tag{8}$$

2.3.4. Centre of mass

Centre of mass is the balance point of an object. It is a position in the object that is assumed to accumulate all of its mass. It makes it easy to work with oddly shaped objects.

$$\boldsymbol{M_x} = \frac{(\sum \boldsymbol{x})}{\boldsymbol{A}} \tag{9}$$

$$\boldsymbol{M_y} = \frac{(\sum y)}{A} \text{ (10).}$$

2.3.5. Moment of inertia

The moment of inertia in physics is a property that opposes the change of state of the object in rotational motion. In image processing it refers to Second-order moments which describe how mass varies around the center of mass.

Moment of inertia xx: $I_{xx} = (\sum x^2) - A^* M_x{}^2$ (11).

Moment of inertia yy: $I_{yy} = (\sum y^2) - A^* M_y{}^2$ (12).

3. Results and discussions

3.1. Image acquisition

The main dataset used in this paper was provided by the Multi-Centre, Multi-Vendor and Multi-Disease Cardiac Segmentation (M&M), organized as part of the Statistical Atlases and Computational Modelling of the Heart (STACOM) Workshop, held in conjunction with

the MICCAI 2020 Conference. (The dataset is publicly available at https://www.ub.edu/mnms).

It was collected from three different countries (Spain, Germany, and Canada), where four different types of scanners were used (Siemens, General Electric, Philips, and Canon). It was gathered from 375 subjects, including patients suffering from hypertrophic and dilated cardiomyopathies and healthy subjects. The training set has 150 annotated images generated by two vendors and 25 unannotated images from a third vendor. The testing set has 200 images, 50 new cases provided by each of the previous vendors, and 50 by a new vendor.

Experienced clinicians provided segmentation and notations of the data from the respective institutions; it included contours of the left (LV) and right ventricle (RV) and left ventricular myocardium (MYO) [37].

3.2. Methodology

Our method is based on human-thinking process: The expert sees the image, recognises it as a long axis or a short axis slice. They would recognise different components by their colour/grey level degree, then differentiate between the different structures using shape, position, and size.

Similarly, we tried to recreate each step with computerized techniques. Fig. 1 shows each step and its computerization.

3.2.1. View identification

The motivation behind this step is that an expert naturally distinguishes between the two views at first sight. A similar approach in automatic localization can help reduce computation cost, as it will use attributes specific to one view per image.

Long-axis and short-axis views are very different, and they can offer different sorts of information. For example, a long-axis view usually contains the four chambers and the aorta, while a short axis view has two chambers. Human experts can easily distinguish between the two views, then recognise different heart chambers accordingly. To mimic the same process, we run a classification step using transfer learning.

Deep learning has been widely used for image classification; the neural networks learn complicated patterns that help fit an image into its suitable class. For this task, we tested a number of pre-trained models and finally settled on a residual network (Resnet) with 101 layers; we kept the weights on all the layers except for the last one and trained the network again.

In order to create data for training and testing, we manually separated the images into long axis and short axis views, following the labelling provided by the original dataset.

Naturally the number of short axis images is significantly higher than long axis images. this is a result of any MRI exam, due to the elongated shape of the heart.

As shown in Table 1 the dataset in hand is quite imbalanced, it contains a larger number of short-axis as opposed to long-axis images, this is due to the nature of an MRI scan and the shape of the heart. Research have been done on the impact of dropout on training with unbalanced data [38], to avoid overfitting, we experienced with dropout and settled on 30% for our final model.

We trained the model for 5 epochs over the whole dataset, for a duration of 1228 min, it achieved a 99 % accuracy. The detailed confusion matrix is shown in Fig. 2. The model has better performance classifying short axis images (99.9%), than long axis images (95.5%). This is due to the abundance of short axis images, not only in the dataset, but in all cardiac MRI exams.

High performance is not unusual in deep learning algorithm, especially when using transfer learning. To ensure the results were valid and not due to overfitting, meaning the model didn't memorize the images by heart but learned how to recognise them properly (a common problem when dealing with small datasets); we have tested the model on unseen images, and it still reported accurate classification. We achieved 98.31% validation accuracy.

3.2.2. Segmentation and localisation of the left and the right ventricles

We applied Particle Swarm Optimization algorithm for the segmentation of the short and long-axis views. We present in Fig. 3 a segmentation example by using the PSO algorithm with 3 clusters.

As shown in Fig. 3.b, the algorithm segments the short axis view into three classes. The first represented by the low intensity pixels, and

Table 1
Description of the classification dataset.

Training images		Test images	
Long axis	Short axis	Long axis	Short axis
1612	6350	323	1270

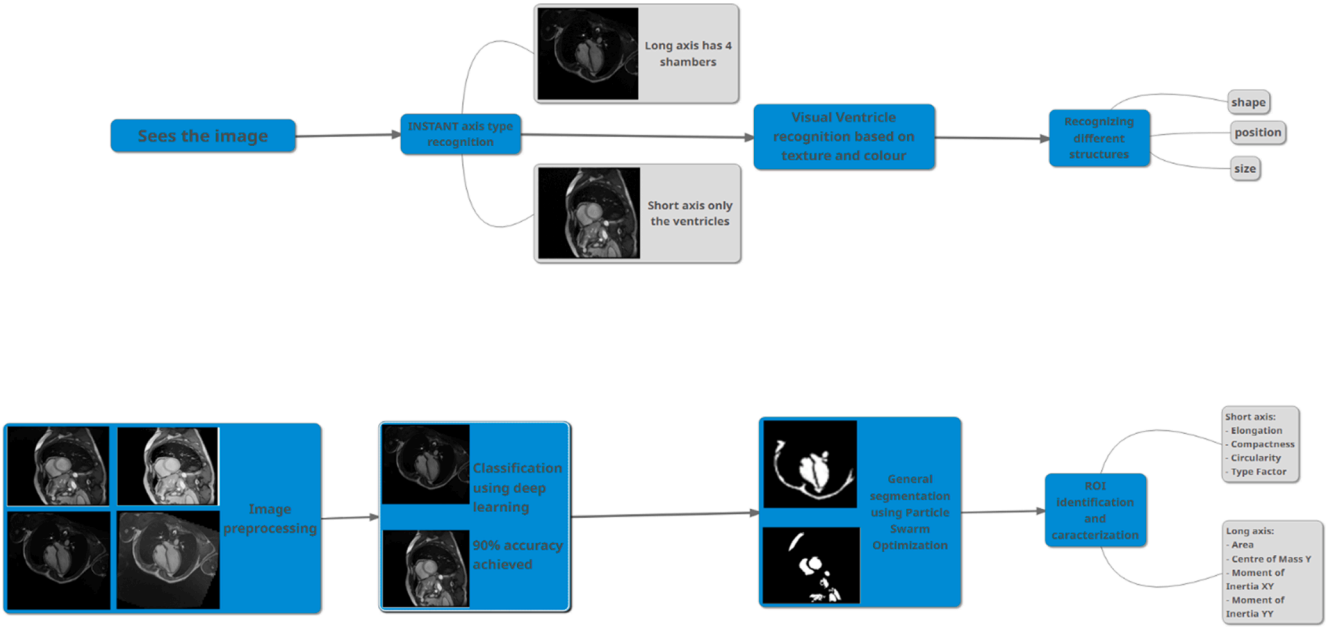

Fig. 1. Thinking process for ventricle identification vs. computerized workflow.

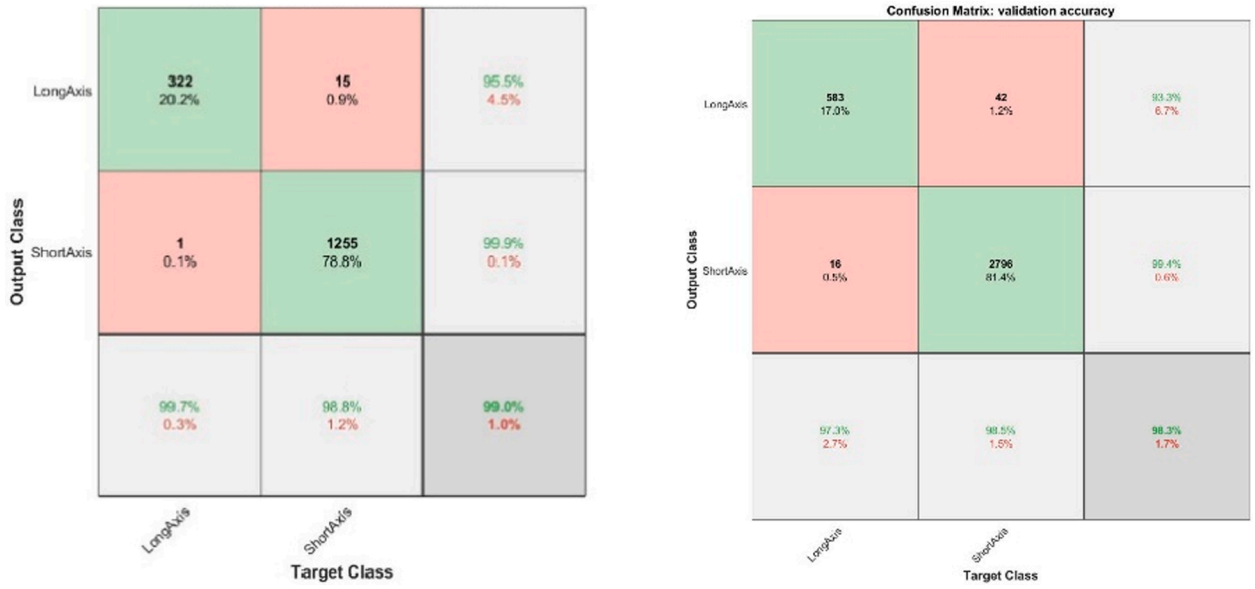

Fig. 2. Confusion Matrices that describe the classification performance in detail On the left is the classification of test images, on the right classification of validation images.

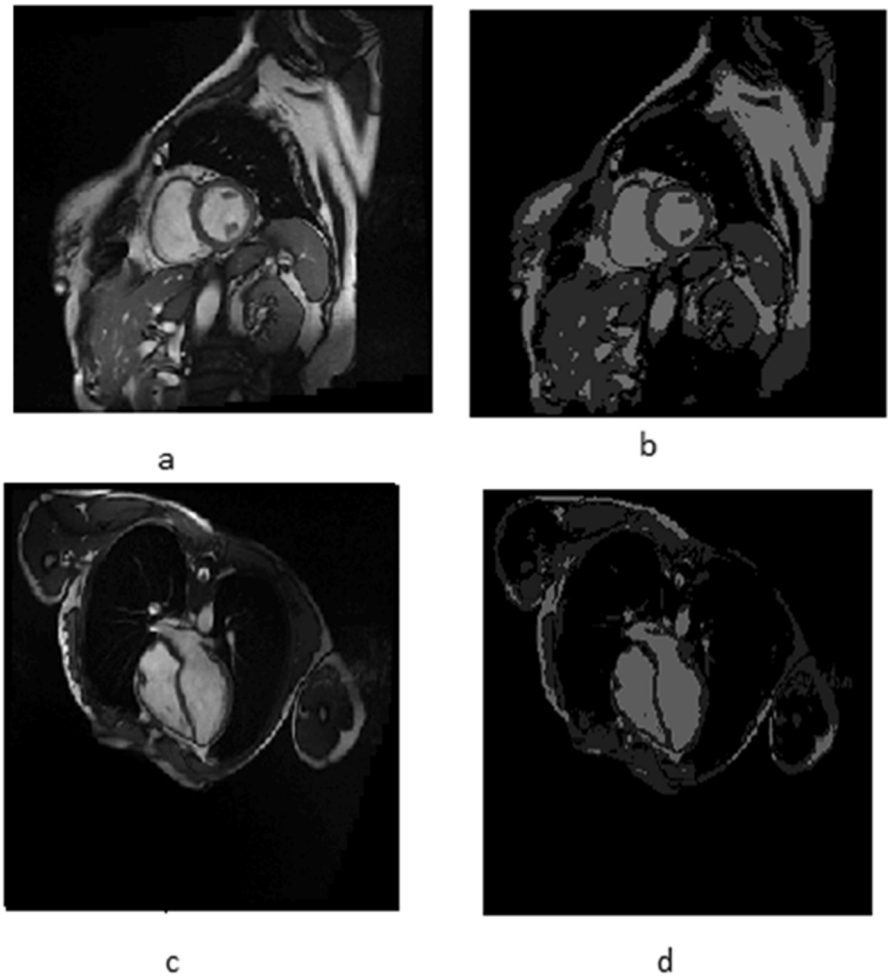

Fig. 3. (a, c) Original images. (b, d) Images after segmentation with PSO.

contains the lung and the background of the image. The second gathers the pixels of average intensities like the myocardium, and the third gathers high intensities like the left and right ventricles.

While for the long axis view (Fig. 3.d), the first cluster represented by the low intensities contains the two lungs and the background. The average intensities like the myocardium represent the second cluster, while the third cluster contains the regions with high intensities like the left atrium, ventricle, right atrium, and descendent aorta.

In our task to localize the left ventricle and right ventricle, we start by detecting the lung from the first class (Fig. 4.e).

Using the detected lung's position, we can consequently detect the right and left ventricles from the third class (Fig. 4.F).

As represented in Fig. 5, we have three regions of interest for the long axis view: the aorta, the left heart (left atrium and ventricle), and the right heart (right atrium and ventricle).

4. Results and discussions

For each image we calculated, using the bounding box method, area.

We used the bounding box method to calculate the following parameters (groups) for each image: area, compactness, elongation factor, circularity factor, type factor, centers of mass X and Y, moments of inertia XX, XY and YY.

ANOVA is used to compare differences of means among more than two groups. It does this by looking at variation in the data and where that variation is found (hence its name). Specifically, ANOVA compares the amount of variation between groups with the amount of variation within groups.

In order to select the most relevant features for ventricle characterization, we used Analysis of variance (ANOVA). ANOVA is a statistical analysis tool that was developed by Ronald Fisher in 1918, it tests whether any difference exists between the groups on some variable (feature) according to the following steps:

- Assume all groups have the same variance (null hypothesis)
- Calculate the Sum of Squares (MST)
- calculate the ANOVA effect size, which determines the degree of freedom (d.f)
- Calculate F-value (equation (13)); an F-test is a way of telling if a group of variables are jointly significant. deciding to support or reject the null hypothesis.

$$F = \frac{MSE}{MST} \tag{13}$$

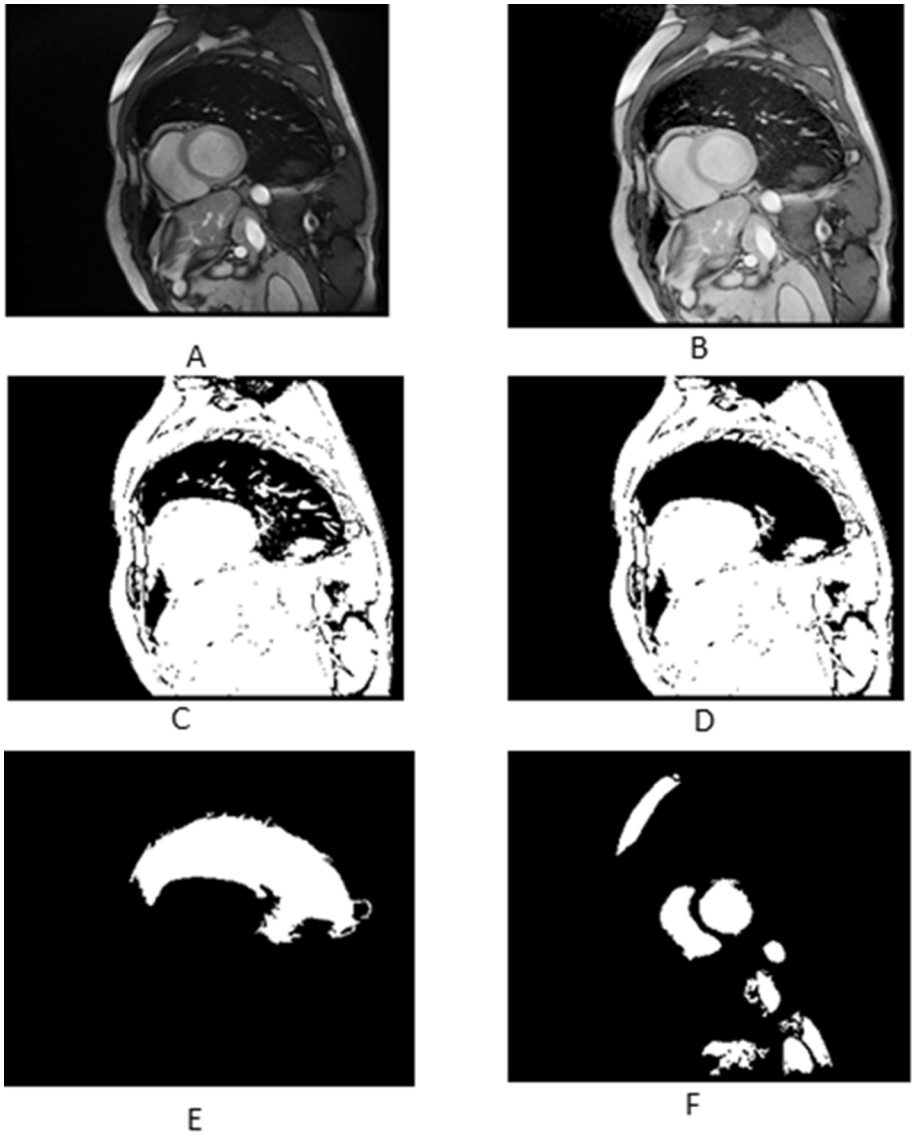

Fig. 4. The different steps of the proposed methodology.

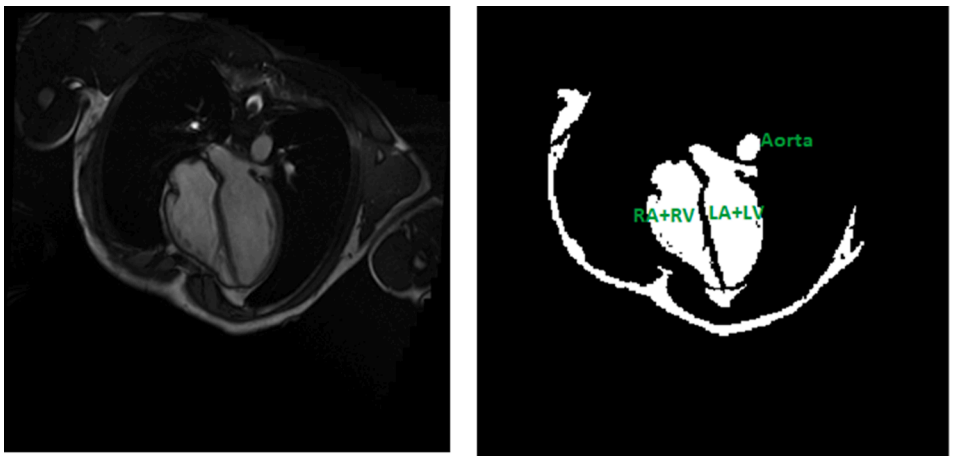

Fig. 5. The segmentation result on a long axis image.

where:
F: ANOVA coefficient.
MST: Mean sum of squares due to treatment.
MSE: Mean sum of squares due to error.

- Accept or Reject the Null Hypothesis

After segmentation, a long-axis view image contains the right heart (the right ventricle + right atrium), the left heart (left atrium + ventricle), and the aorta. We picked 8 different features that can characterize the different groups, then we tested for the most significant features.

Table 2 demonstrates the detailed process of testing the features, while Fig. 5 shows the ANOVA representations. In the table we provided every feature we tested, sum square, degree of freedom, mean square, f-value, and the final verdict based on the comparison between the f value and the F critical value.

Fig. 6 provides a more visible interpretation of the interactions between the different groups. For a specific feature, when there is no overlap between two structures, the feature is considered a good criteria to distinguish between the two structures.

Not all the features studied above have significant "variation", and can be for classification.

To be accurate only two features were good enough for our evaluation: centre of mass Y, and area. Position could also be used to tell the left heart and the right heart apart, but we haven't used spatial features in this work due to the non-consistency if the dataset. This will definitely be explored in a future work.

Table 2
Feature extraction for long axis segmentation.

	source	Sum square	Degree of freedom	Mean square	F-value	Prb > f	Verdict
Centre of Mass X	g	8221	3	2470.34	1.04	0.3857	Feature not significant
	error	10,549	40	2637.3			
	Total	113,713	43				
Centre of Mass Y	g	27859.5	3	9286.5	8.6	**0.0002**	The aorta is significantly different from every other group
	error	43202.4	40	1080.06			
	Total	71061.9	43				
Area	g	5.4749 10^{07}	3	1.82497 10^{07}	6.05	0.0017	Left heart and right heart are different than other groups
	Error	1.20749 10^{08}	40	3.01872 10^{06}			
	Total	1.75498 10^{08}	43				
Elongation Factor	g	15.7963	3	5.26542	5.74	0.0023	Feature not significant
	Error	36.7085	40	0.91771			
	Total	52.5048	43				
Heywood Circularity Factor	g	3.519	3	1.17301	4.29	0.0102	Feature not significant
	Error	10.9277	40	0.27319			
	Total	14.4468	43				
Moment of Inertia XX	g	6.97888 10^{12}	3	2.32629 10^{12}	1.59	0.2061	Feature not significant
	Error	5.84062 10^{13}	40	1.46015 10^{12}			
	Total	6.5351 10^{13}	43				
Moment of Inertia XY	g	6.7484 10^{12}	3	2.24947 10^{12}	3.45	0.0253	Can be used to identify left heart
	Error	2.60511 10^{13}	40	6.51278 10^{11}			
	Total	3.27995 10^{13}	43				
Moment of Inertia YY	g	6.7484 10^{12}	3	2.24947 10^{12}	3.45	0.0253	Can be used to identify left heart
	Error	2.60511 10^{13}	40	6.51278 10^{11}			
	Total	3.27995 10^{13}	43				

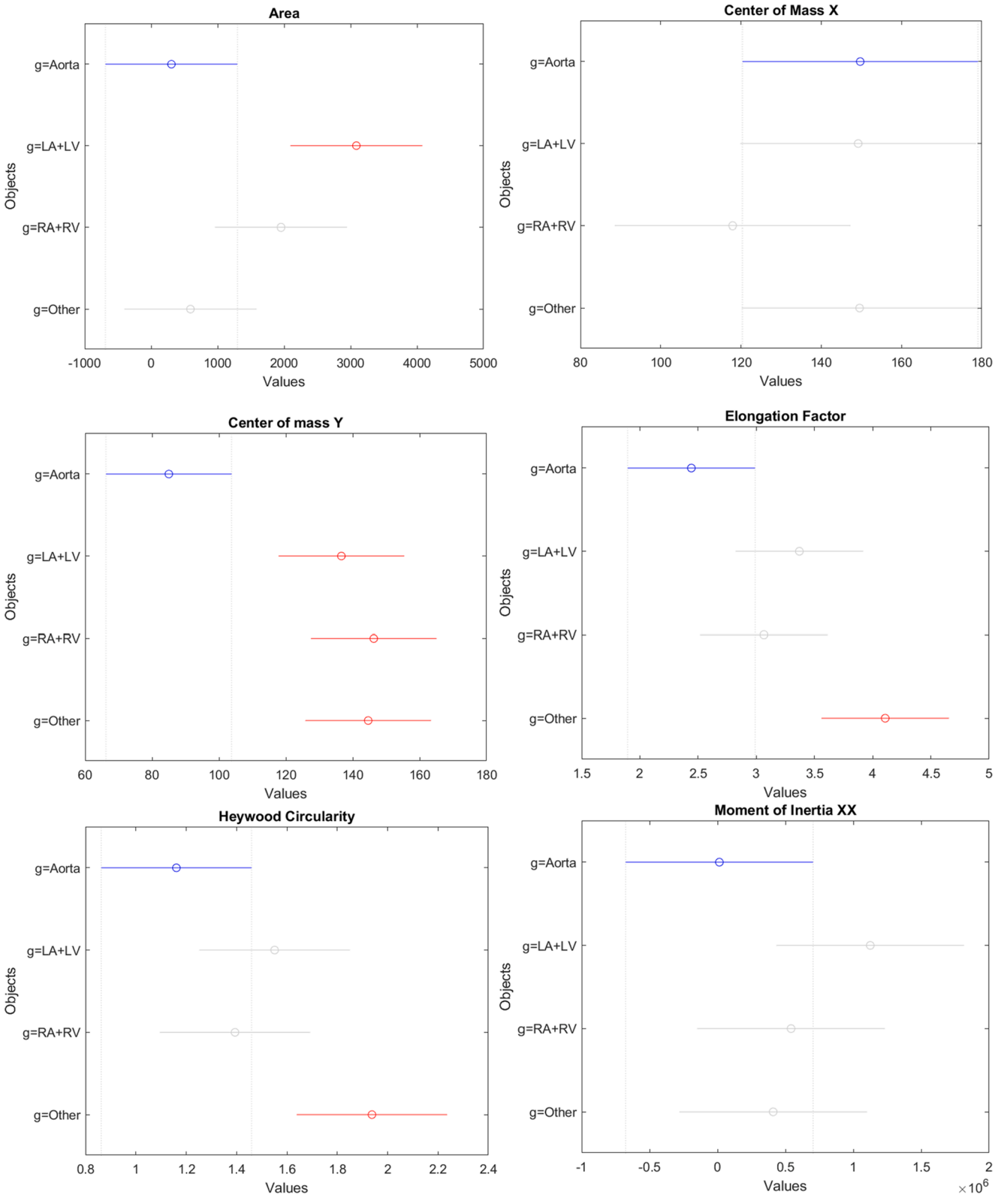

Fig. 6. ANOVA representations of the long-axis features.

The aorta has a significantly lower centre of mass Y with F-value = 0.0002 compared to the other objects on the segmented image. At the same time, the left heart has a higher moment of inertia XY moment of inertia YY compared to the other objects.

In the same fashion, Table 3 and Fig. 7 contain features we tested for short axis characterization.

All four features tested in Table 3 and Fig. 7 can be used to characterize and distinguish between the right and left ventricles on short-axis images. The right ventricle has high elongation and Heywood circularity, while the left ventricle can be characterized with high compactness and type factor.

Table 3
Feature extraction for short axis segmentation.

	Source	Sum square	Degree of freedom	Mean sq.	F-value	Prb > f	Verdict
Elongation	g	7.7261	1	7.72607	66.58	$7.03777\ 10^{-10}$	Significant feature
	error	4.4094	38	0.11604			
	Total	12.1355	39				
Compactness	g	0.20517	1	0.20517	64.61	$1.01530\ 10^{-09}$	Significant feature
	error	0.12067	38	0.00318			
	Total	0.32584	39				
Heywood Circularity	g	0.5774	1	0.5774	42.74	$1.04602\ 10^{-07}$	Significant feature
	Error	0.51339	38	0.01351			
	Total	1.0908	39				
Type Factor	g	0.42483	1	0.42483	155.14	$5.47648\ 10^{-15}$	Significant feature
	Error	0.10406	38	0.00274			
	Total	0.52889	39				

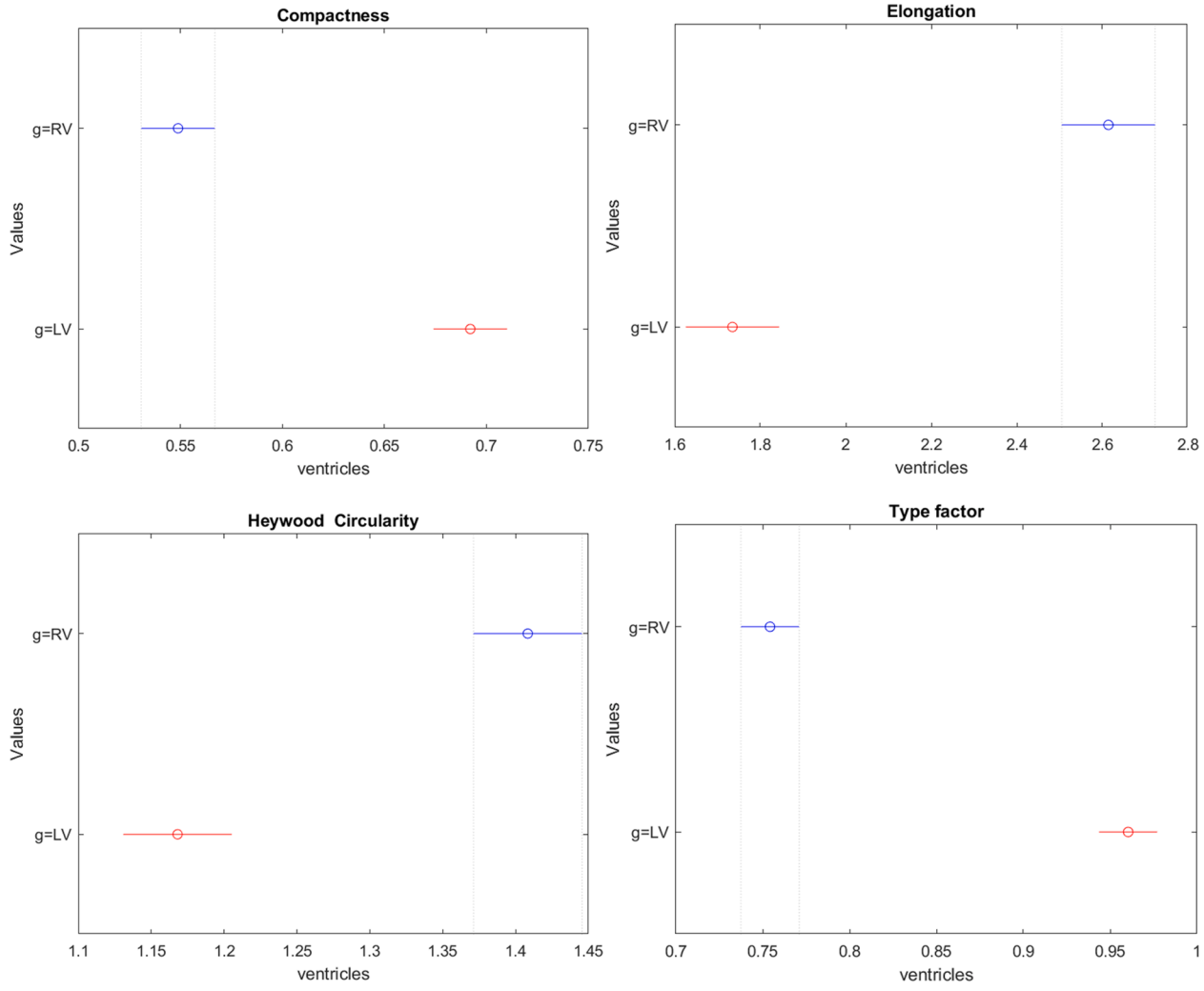

Fig. 7. ANOVA representations of the short-axis features.

5. Conclusion

In recent computer vision solutions, explainability has become an urging concern especially in medical applications. it is crucial for clinicians to understand the process behind the result, which is not always possible when extracting the information straight from the provided images, that is why this work has focused on achieving segmentation and characterization of structures of interest in cardiac MRI images following a detailed workflow. We tried to make the process explainable by imitating a human-like workflow, then automating every step.

A human expert would recognize the images as long axis or short axis slices from first sight; accordingly, they would know what to expect to find in the image. They would recognize left ventricle based on its circular shape, right ventricle based on its lunar shape, and the lung based on its position; In this paper we recreated the same workflow but with computerizing each step.

We began by classifying the images into long-axis and short-axis views first, which allows a more customised segmentation and

processing of the images. We could successfully achieve 99% classification accuracy using a pre-trained Resnet model. It is not uncommon for pre-trained models to achieve high performance even with little data, which was the reason we used it to compensate for the relatively small dataset.

We used Particle Swarm Optimization (PSO) for general segmentation, the algorithm has gained popularity for creating segments with good attention to details. PSO was applied to all images equally because the textures of the structures do not change from one view to another.

In order to identify the different objects present after segmentation, we tested a number of descriptors including area, centre of mass, circularity and elongation factors, moment of inertia. ANOVA was used for feature selection to detect the location of each region of interest.

Short axis images were easier to deal with, as they only have three regions of interest: lung, left ventricle and short ventricle; all three structures are significantly different. The lung could be easily identified based on its large area and removed. As for the right and left ventricle, they could be each located based on: elongation, compactness, Heywood circularity, and type factor.

Long axis images, however, contain all four chambers, plus the aorta and other structures. To make our work simpler, we considered the regions of interest to be: aorta, left heart (left ventricle + left atrium), right heart (right ventricle + right atrium), and other. Having so many groups with similar attributes made the process of feature selection more complicated; the aorta was easily identified by.

The purpose of such characterization is to provide a tool that eventually allows advanced segmentation locating objects of interest after a global segmentation using classification methods: FCM, KFCM, EM and operator's manual and automatic thresholding.

This was an initial study to test the possibility of applying a human-inspired workflow with computerizing every step, as an attempt to have an explainable fully automatic segmentation of cardiac structures. Even though the process seems long, it was rather simple to apply. Applying the classification step would mean we'd only use one set of attributes to characterize the segmented structures, this can be cost efficient.

At last, it is important to note that the innovation of our work isn't the models used at each step, but the workflow itself; recreating a human-like thinking process is what we are aiming for.

Further work will be done in the future to perfect the outcome of every step, which should have good results considering the advances provided in the literature for each step (classification, segmentation, feature selection).

CRediT authorship contribution statement

Laidi Amel: Conceptualization, Methodology, Software, Data curation, Writing – original draft. **Mohammed Ammar:** Supervision, Conceptualization. **Mostafa El Habib Daho:** Visualization, Investigation. **Said Mahmoudi:** .

Declaration of Competing Interest

The authors declare that they have no known competing financial interests or personal relationships that could have appeared to influence the work reported in this paper.

References

[1] A. Pednekar, U. Kurkure, R. Muthupillai, S. Flamm, I.A. Kakadiaris, Automated left ventricular segmentation in cardiac MRI, IEEE Trans. Biomed. Eng. 53 (7) (2006) 1425–1428.

[2] J. Huang, X. Huang, D. Metaxas, L. Axel, Dynamic Texture based Heart Localization and Segmentation in 4-D Cardiac Images, in: 2007 4th IEEE International Symposium on Biomedical Imaging: From Nano to Macro, 2007, pp. 852–855.

[3] M.-P. Jolly, Automatic recovery of the left ventricular blood pool in cardiac cine MR images. in *nternational Conference on Medical Image Computing and Computer-Assisted Intervention*, 2008.

[4] C. Constantinides, Y. Chenoune, E. Mousseaux, E. Roullot, F. Frouin, Automated heart localization for the segmentation of the ventricular cavities on cine magnetic resonance images. in *2010 Computing in Cardiology*, 2010.

[5] S.-K. Pavani, D. Delgado, A.F. Frangi, Haar-like features with optimally weighted rectangles for rapid object detection, Pattern Recogn. 43 (1) (2010) 160–172.

[6] S. Huang, J. Liu, L.C. Lee, S.K. Venkatesh, L.L.S. Teo, C. Au, W.L. Nowinski, An image-based comprehensive approach for automatic segmentation of left ventricle from cardiac short axis cine MR images, J. Digit. Imaging 24 (4) (2011) 598–608.

[7] Y.-L. Lu, K.A. Connelly, A.J. Dick, G.A. Wright, P.E. Radau, Automatic functional analysis of left ventricle in cardiac cine MRI, Quantitative imaging in medicine and surgery 3 (4) (2013) 200.

[8] M. Ammar, S. Mahmoudi, M.A. Chikh, A. Abbou, Endocardial border detection in cardiac magnetic resonance images using level set method, J. Digit. Imaging 25 (2) (2012) 294–306.

[9] U. Kurkure, A. Pednekar, R. Muthupillai, S.D. Flamm, I.A. Kakadiaris, Localization and segmentation of left ventricle in cardiac cine-MR images, IEEE Trans. Biomed. Eng. 56 (5) (2008) 1360–1370.

[10] A. Pednekar, I. A. Kakadiaris, V. Zavaletta, R. Muthupillai and S. Flamm, "Automatic hybrid segmentation of dual contrast cardiac MR data," in *International Conference on Medical Image Computing and Computer-Assisted Intervention*, Berlin, Heidelberg, 2002.

[11] C. Pluempitiwiriyawej, J.M.F. Moura, Y.-J.-L. Wu, C. Ho, Cardiac MR image segmentation: Quality assessment of STACS. in *2nd IEEE International Symposium on Biomedical Imaging: Nano to Macro*, 2004.

[12] D. Grosgeorge, C. Petitjean, J.-N. Dacher, S. Ruan, Graph cut segmentation with a statistical shape model in cardiac MRI, Comput. Vis. Image Underst. 117 (9) (2013) 1027–1035.

[13] D. Mahapatra, J.M. Buhmann, Automatic cardiac RV segmentation using semantic information with graph cuts. in *IEEE 10th International Symposium on Biomedical Imaging*, 2013.

[14] M.C.F.X.P. Sermesant, H. Delingette, N. Ayache, Deformable biomechanical models: application to 4d cardiac image analysis, Med. Image Anal. 7 (4) (2003) 475–488.

[15] C. Petitjean, M.A. Zuluaga, W. Bai, J.-N. Dacher, D. Grosgeorge, J. Caudron, S. Ruan, I.B. Ayed, M.J. Cardoso, H.-C. Chen, D. Jimenez-Carretero, M.J. Ledesma-Carbayo, C. Davatzikos, Jimit, Right ventricle segmentation from cardiac MRI: A collation study, Med. Image Anal. 19 (2015) 187–202.

[16] J. Peters, O. Ecabert, C. Meyer, H. Schramm, R. Kneser, A. Groth, J. Weese, Automatic whole heart segmentation in static magnetic resonance image volumes. in *International Conference on Medical Image Computing and Computer-Assisted Intervention*, 2007.

[17] M. Lorenzo-Valdés, G.I. Sanchez-Ortiz, A.G. Elkington, R.H. Mohiaddin, D. Rueckert, Segmentation of 4D cardiac MR images using a probabilistic atlas and the EM algorithm, Med. Image Anal. 8 (3) (2004) 255–265.

[18] W. Bai, W. Shi, D.P. O'regan, T. Tong, H. Wang, S. Jamil-Copley, N.S. Peters, D. Rueckert, A probabilistic patch-based label fusion model for multi-atlas segmentation with registration refinement: application to cardiac MR images. in *IEEE transactions on medical imaging*, 2017.

[19] C. Chen, C. Qin, H. Qiu, G. Tarroni, J. Duan, W. Ba, D. Rueckert, Deep Learning for Cardiac Image Segmentation: A Review, Frontiers in Cardiovascular Medicine 7 (2020) 25.

[20] T.A. Ngo, Z. Lu, G. Carneiro, Combining deep learning and level set for the automated segmentation of the left ventricle of the heart from cardiac cine magnetic resonance, Med. Image Anal. 35 (2017) 159–171.

[21] N. Otsu, A threshold selection method from gray-level histograms, IEEE transactions on systems, man, and cybernetics 91 (1979) 62–66.

[22] T.A. Ngo, G. Carneiro, "Fully automated segmentation using distance regularised level set and deep-structured learning and inference", in *Deep Learning and Convolutional Neural Networks for Medical Image Computing*, Springer (2017) 197–224.

[23] M.R. Avendi, A. Kheradvar, H. Jafarkhani, A combined deep-learning and deformable-model approach to fully automatic segmentation of the left ventricle in cardiac mri, Med. Image Anal. 30 (2016) 108–119.

[24] G.S.D.K.W. Luo, H. Zhang, Cardiac left ventricular volumes prediction method based on atlas location and deep learning. in *IEEE International Conference on Bioinformatics and Biomedicine (BIBM)*, 2016.

[25] C. Rupprecht, E. Huaroc, M. Baust, N. Navab, Deep Active Contours, ArXiv (2016).

[26] M.-M. Rohé, M. Sermesant, X. Pennec, Automatic Multi-Atlas Segmentation of Myocardium with SVF-Net. in *International Workshop on Statistical Atlases and Computational Models of the Heart*, 2017.

[27] M.-M. Rohé, M. Datar, T. Heimann, M. Sermesant, X. Pennec, SVF-Net: Learning Deformable Image Registration Using Shape Matching. in *International conference on medical image computing and computer-assisted intervention*, 2017.

[28] H. Yang, J. Sun, H. Li, L. Wang, Z. Xu, Neural multi-atlas label fusion: Application to cardiac MR images, Med. Image Anal. 49 (2018) 60–75.

[29] Z. Wang, Automatic Localization and Segmentation of the ventricles in magnetic resonance images, IEEE Trans. Circuits Syst. Video Technol. 31 (2) (2020) 621–631.

[30] J. M. Noothout, B. D. de Vos, J. M. Wolterink, T. Leiner and I. Išgum, "CNN-based landmark detection in cardiac CTA scans," *arXiv preprint arXiv:1804.04963,* 2018.

[31] D. Mahapatra, Landmark detection in cardiac MRI using learned local image statistics. in *International Workshop on Statistical Atlases and Computational Models of the Heart*, 2012.

[32] P. Ghamisi, M.S. Couceiro, J.A. Benediktsson, Extending the fractional order Darwinian particle swarm optimization to segmentation of hyperspectral images. in *Image and Signal Processing for Remote Sensing XVIII*, 2012.

[33] X. Song, H. Li, Segmentation Based on Particle Swarm Optimization. in *International Conference on Applications and Techniques in Cyber Security and Intelligence*, 2020.
[34] T.R. Farshi, J.H. Drake, E. Özcanc, A multimodal particle swarm optimization-based approach for image segmentation, Expert Syst. Appl. 149 (2020), 113233.
[35] P. Ghamisi, M.S. Couceiro, F.ML. Martins, J.A. Benediktsson, Multilevel Image Segmentation Based on Fractional-Order Darwinian ParticleSwarm Optimization, IEEE Trans. Geosci. Remote Sens. 52 (5) (2013) 2382–2394.
[36] M. Ammar, M. Saïd, M.A. Chikh, A. Abbou, Toward an Automatic Left Atrium Localization Based on Shape Descriptors and Prior Knowledge. in *International Workshop on Statistical Atlases and Computational Models of the Heart*, 2013.
[37] V. M. Campello, P. Gkontra, C. Izquierdo, C. Martın-Isla, A. Sojoudi, P. M. Full, K. Maier-Hein, Y. Zhang, Z. He, J. Ma, M. Parreno, A. Albiol, F. Kong, S. C. Shadden, J. C. Acero and others, "Multi-centre, multi-vendor and multi-disease cardiac segmentation: The m&ms challenge," *IEEE Transactions on Medical Imaging,* vol. 40, no. 12, pp. 3543–3554, 2021.
[38] R. Dabare, K. W. Wong, P. Koutsakis and M. F. Shiratuddin, "A Study of the Effect of Dropout on Imbalanced Data Classification using Deep Neural Networks," *Journal of Multidisciplinary Engineering Science and Technology (JMEST),* vol. 5, 2018.